AIAA JOURNAL
Vol. 42, No. 5, May 2004

Low-Aspect-Ratio Wing Aerodynamics at Low Reynolds Numbers

Gabriel E. Torres* and Thomas J. Mueller†
University of Notre Dame, Notre Dame, Indiana 46556

The recent interest in the development of small unmanned aerial vehicles (UAVs) and micro air vehicles has revealed a need for a more thorough understanding of the aerodynamics of small airplanes flying at low speeds. In response to this need, a study of the lift, drag, and pitching moment characteristics of wings of low aspect ratio operating at low Reynolds numbers are presented. Wind-tunnel tests of wings with aspect ratios between 0.5 and 2.0, four distinct planforms, thickness-to-chord ratios of $\approx 2\%$, and 5-to-1 elliptical leading edges have been conducted as part of this research. The Reynolds numbers considered were in the range of 7×10^4 to 2×10^5. Analysis of the data includes comparison of lift-curve slope, nonlinear equation approximations, maximum lift coefficient, and center of lift.

Nomenclature

AR	=	aspect ratio, b^2/S
b	=	wing span
C_D	=	drag coefficient, $D/\frac{1}{2}\rho {V_\infty}^2 S$
C_{D_0}	=	drag coefficient at zero lift
C_L	=	lift coefficient, $L/\frac{1}{2}\rho {V_\infty}^2 S$
$C_{L_{\max}}$	=	maximum lift coefficient
C_{L_α}	=	three-dimensional lift-curve slope, 1/deg
C_{l_α}	=	two-dimensional lift-curve slope, 1/rad
C_M	=	pitching moment coefficient about $\bar{c}/4$, $M/\frac{1}{2}\rho {V_\infty}^2 S\bar{c}$
C_{root}	=	root chord
c	=	wing chord
$\bar{c}$	=	mean aerodynamic chord
D	=	drag force
h_{CL}	=	nondimensional location of center of lift, $x_{\text{CL}}/\bar{c}$
K	=	induced drag factor
K_p	=	potential component of lift for Polhamus/Lamar approximation
K_v	=	vortex (nonlinear) component of lift for Polhamus/Lamar approximation
L	=	lift force
Re	=	Reynolds number based on wing root chord, $\rho V_\infty C_{\text{root}}/\mu$
S	=	wing area
V_∞	=	freestream velocity
x_{CL}	=	chordwise location of center of lift
$x_{\bar{c}/4}$	=	chordwise location of $\bar{c}/4$
x_e	=	chordwise location for leading-edge and side-edge vortex forces
x_p	=	chordwise location for potential force
α	=	angle of attack, deg
$\alpha_{C_{L_{\max}}}$	=	angle of attack at maximum lift
Δy	=	leading-edge shape parameter
η	=	airfoil lift-curve slope efficiency parameter
$\Lambda_{c/2}$	=	sweep angle at half-chord
μ	=	viscosity
ρ	=	air density
τ	=	Glauert efficiency parameter

Received 9 January 2003; revision received 4 December 2003; accepted for publication 13 January 2004.

*Research Assistant, Department of Aerospace and Mechanical Engineer, Hessert Laboratory for Aerospace Research; currently Aerospace Engineer, AeroVironment, Inc., Design Development Center, 4685-3H Industrial Street, Simi Valley, CA 93063.

†Roth-Gibson Professor, Department of Aerospace and Mechanical Engineering, Hessert Laboratory for Aerospace Research. Fellow AIAA.

I. Introduction

A GREAT deal of interest has emerged during the last several years for a totally new kind of unmanned aerial vehicle (UAV). Although large unmanned aircraft have proven to be successful as theater-level military reconnaissance platforms, a need for a smaller, platoon-level unmanned aircraft exists. Small UAVs such as the Pointer, Sender, and, more recently, the Dragon Eye[1] and Raven,[2] have fulfilled this need. An even smaller alternative is the micro air vehicle (MAV). MAVs are small, remotely piloted aircraft slated to be used for close-range reconnaissance or sensing missions. Some of the goals for MAVs are[3] as follows maximum dimension of 15 cm (6 in.), operating range of 10 km (6.2 miles), average endurance of 30 min, payload capability up to 18 g (0.63 oz), and autonomous or semiautonomous control. Although recent MAV designs[4–7] have shown that it is possible to make operational vehicles that are small and can carry a payload in the order of 20 g, it has been recognized that such a small payload limits the types of missions these airplanes can perform. In response to this, there is now a greater interest in slightly larger MAVs that can carry larger payloads (in the form of sensors, autopilots, or global positioning system (GPS) navigation, as well as more fuel or energy storage for greater endurance/range).

The design of efficient MAVs is hindered, however, by the lack of a thorough understanding of the aerodynamics associated with low-aspect-ratio wings (usually AR below two) operating at low Reynolds numbers (roughly between 7×10^4 and 2×10^5). Classical aerodynamic theory, although accurate for full-scale aircraft analysis, is found to be inadequate for this combination of aspect ratio and Reynolds number. Furthermore, wings with low aspect ratios exhibit unique aerodynamic properties, such as high values of $\alpha_{C_{L_{\max}}}$ and nonlinear lift vs angle of attack. A need exists for detailed aerodynamic analysis tools that are applicable to the Reynolds number and aspect ratio operating conditions found in MAVs and in some small UAVs.

A thorough literature survey has revealed that only a small number of researchers have addressed this need. (See, for instance, Refs. 8–17.) Most of these works, however, focus on low-aspect-ratio (LAR) wings at higher Reynolds numbers.

In terms of the theory of LAR wing aerodynamics, much work has been performed in an attempt to model the nonlinear lift of LAR wings mathematically. Many approaches focus on empirically based modifications of linear theory through the addition of α^2 or $\sin^2\alpha$ terms. More detailed studies propose a modified version of Prandtl's lifting-line theory[18,19] and an analogy to the leading-edge suction as a source of nonlinear lift.[20–23]

The lift mechanisms of LAR wings can be summarized in terms of two additive sources of lift: a linear and a nonlinear source. The linear lift can be modeled by the existence of circulation around the airfoil and is what is typically thought of as lift in higher AR wings. Nonlinear lift arises from the existence of strong wingtip vortices, which generate strong cross-flow velocities on the upper surface of the wing. The ensuing decrease in pressure is considered to be the main source of nonlinear lift of LAR wings at moderate to high angles of attack.

Reynolds number effects also play a dominant role in the aerodynamics of MAVs and small UAVs. As the Reynolds number decreases, the overall performance of a lifting body decreases. Phenomena such as separation bubbles (which can be as large as 20–30% of the chord) can significantly affect lift and drag characteristics. In some cases, separation bubbles may lead to an effective increase in the camber of the wing or may act as a trip for earlier transition than would occur at higher Reynolds numbers where the bubble is not present.

It is the goal of this paper to provide aerodynamic data corresponding to LAR wings at low Reynolds numbers for the purpose of supporting the analysis of small aircraft operating at low speeds. The data are based on wind-tunnel experiments of flat-plate wings of 2% thickness with aspect ratios between 0.5 and 2.0 and four distinct planforms. Discussion of the data includes identification of key performance parameters, such as lift-curve slope, drag characteristics, comparison with nonlinear lift theories, maximum lift coefficient and corresponding angle of attack, and location of the center of lift.

II. Experimental Apparatus and Procedures

A. Wing Models

The main objective of the present study is to determine the aerodynamic characteristics of LAR wings as influenced by the following three principal factors: 1) wing planform, 2) aspect ratio, and 3) Reynolds number. To study the effect of wing planform, four distinct geometries were chosen (rectangular, Zimmerman, inverse Zimmerman, and elliptical).[24] The Zimmerman and inverse Zimmerman planforms are based on the wingtip shapes designed by Zimmerman[25] in the early 1930s and consist of two half-ellipses joined at either the quarter-root-chord location or at the three-quarter-root-chord location.

For each of the four planforms, a total of seven aspect ratio values were tested, varying from 0.50 to 2.00 in increments of 0.25. This range of aspect ratios was chosen because many of the current implementations of MAV and small UAV designs have values of AR within this range. Figure 1 shows a schematic of all of the wings tested in wind-tunnel experiments.

The models were constructed from either aluminum or molded resin, had thickness-to-chord ratios between 1.96 and 2.60% (based on the root-chord length), and 5-to-1 elliptical leading and trailing edges. The leading-edge shape parameter Δy has a value of 0.74% of the root chord for this type of leading edge. The rectangular planforms have flat side edges and elliptical leading and trailing edges, whereas the nonrectangular planforms have elliptical edges around the entire model. The leading edge is a critical parameter in wings operating at low Reynolds numbers. Even slight variations in leading-edge shape can have large effects on the aerodynamic forces, especially in terms of the moment coefficient.[24] Leading-edge geometries of the wing models used in these experiments are accurate within +0.0001 in. and −0.0070 in. Table 1 lists the dimensions and other geometry parameters for the wings used in this study. Note that $x_{\bar{c}/4}$ is the distance between the leading edge of the root chord and the 25% point of the mean aerodynamic chord (MAC).

Note that all of the models have 0% camber (flat-plate airfoils). This value of camber was chosen such that a baseline for performance of LAR wings at low Reynolds number could be developed. The performance of cambered wings could then be treated as an incremental effect that is appended to the baseline data for flat-plate wings.

Table 1 Wing dimensions[a]

AR	C_{root}, in.	Span, in.	Area, in.^{2}	$\bar{c}$, in.	$x_{\bar{c}/4}$, in.
		Rectangular planform			
0.50	8.000	4.000	32.000	8.000	2.000
0.75	8.000	6.000	48.000	8.000	2.000
1.00	8.000	8.000	64.000	8.000	2.000
1.25	6.000	7.500	45.000	6.000	1.500
1.50	6.000	9.000	54.000	6.000	1.500
1.75	6.000	10.500	63.000	6.000	1.500
2.00	6.000	12.000	72.000	6.000	1.500
		Zimmerman planform			
0.50	8.000	3.142	19.739	6.791	0.552
0.75	8.000	4.712	29.609	6.791	0.552
1.00	8.000	6.283	39.478	6.791	0.552
1.25	8.000	7.854	49.348	6.791	0.552
1.50	8.000	9.425	59.218	6.791	0.552
1.75	8.000	10.996	69.087	6.791	0.552
2.00	8.000	12.566	78.957	6.791	0.552
		Inverse Zimmerman planform			
0.50	8.000	3.142	19.739	6.791	1.157
0.75	8.000	4.712	29.609	6.791	1.157
1.00	8.000	6.283	39.478	6.791	1.157
1.25	8.000	7.854	49.348	6.791	1.157
1.50	8.000	9.425	59.218	6.791	1.157
1.75	8.000	10.996	69.087	6.791	1.157
2.00	8.000	12.566	78.957	6.791	1.157
		Elliptical planform			
0.50	8.000	3.142	19.739	6.791	0.855
0.75	8.000	4.712	29.609	6.791	0.855
1.00	8.000	6.283	39.478	6.791	0.855
1.25	8.000	7.854	49.348	6.791	0.855
1.50	8.000	9.425	59.218	6.791	0.855
1.75	8.000	10.996	69.087	6.791	0.855
2.00	8.000	12.566	78.957	6.791	0.855

[a]All models have zero camber and thickness of 5/32 in. The thickness-to-root-chord ratio is 1.96% for the 8-in. chord models and 2.60% for the 6-in.-chord models.

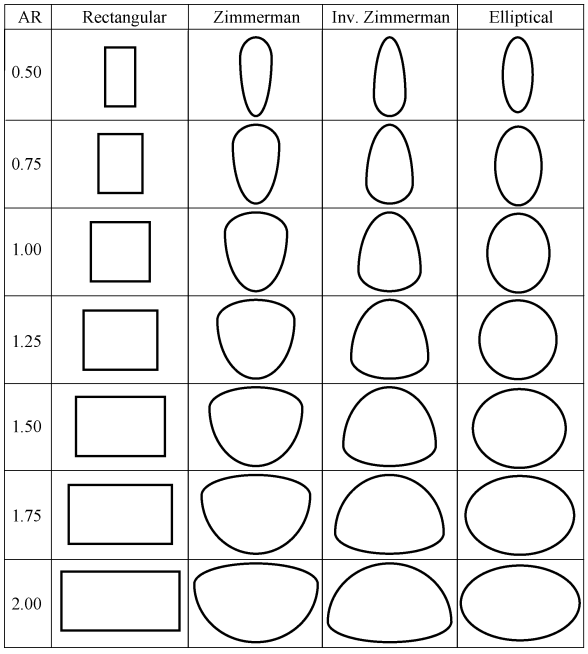

Fig. 1 Wing models used in experiments.

B. Wind Tunnel and Force Balances

All experiments were performed with a low-turbulence, indraft, open-circuit wind tunnel located at the University of Notre Dame's Hessert Laboratory for Aerospace Research. This wind tunnel has a contraction ratio of 20.6 to 1 and a rectangular inlet contraction cone designed specifically for low-turbulence intensities. Over the speed range used for most experiments, the freestream turbulence intensity in the test section was measured to be less

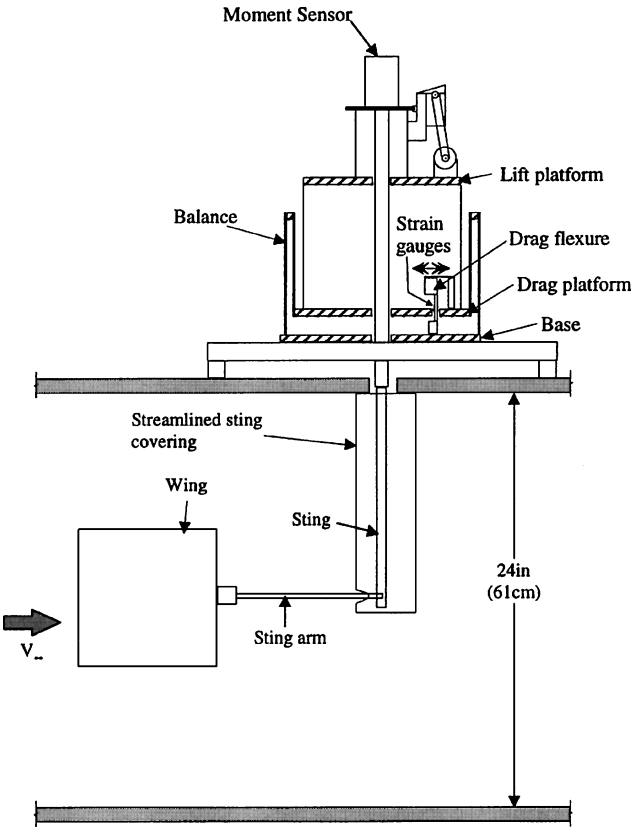

Fig. 2 Mounting of wing models with platform force balance.

than 0.05%. The test section used in all experiments is 6 ft long (1.82 m) with a square cross-sectional area of 2 ft × 2 ft (61 cm × 61 cm).

Lift and drag measurements were made with an especially designed two-component platform force balance that can measure lift and drag forces of wing models down to a chord-Reynolds number of approximately 2×10^4. Normal force and pitching moment were measured by the use of a five-component internal sting balance. (See Torres[24] for details.) The models were mounted with a sting in the trailing edge. The wind-tunnel test setup for lift and drag measurements is shown in Fig. 2. Support interference studies revealed that the sting covering affected the measured aerodynamic forces slightly. The length of the sting arm was optimized to give the least possible interference with the sting covering while keeping the leading edge of the wing far enough from the side walls of the tunnel at high angles of attack.

C. Experimental Procedures and Uncertainty

The angle of attack of the wing models was varied from $\alpha = -10$ deg to either $\alpha = 40$ deg (for wings of $AR \geq 1.50$) or $\alpha = 50$ deg (for wings of $AR \leq 1.25$). The range of α was adjusted whenever possible to measure $\alpha_{C_{L_{\max}}}$. The wings were then brought back to $\alpha = 0$ deg to determine whether hysteresis was present. No hysteresis was observed in any of the measurements.

Lift and drag are nondimensionalized by the area of the wing and the measured dynamic pressure at each angle of attack. Pitching moment was determined from sting balance measurements and is reported at the quarter-chord location of the mean aerodynamic chord of each wing. It is nondimensionalized by the wing area, the dynamic pressure, and the MAC of the wing.

Note that for the analysis in Sec. III.C, the moment coefficient was transposed to the leading edge by addition of the contributions of the lift and drag coefficients. Unless otherwise noted, moment measurements should be taken to be at the quarter chord of the MAC.

Force and moment coefficients presented in this work have all been corrected for wind-tunnel blockage (solid blockage, wake blockage and streamline curvature) according to the techniques presented by Pankhurst and Holder[26] and Barlow et al.[27] The magnitude of the blockage effects varies depending on the size of the wing model, the wing's aspect ratio, and the angle of attack. The largest blockage corrections were found to correspond generally to wings of aspect ratio 2.00 at angles of attack near stall. For these extreme cases, the blockage correction factors for lift, drag, and moment coefficients are approximately 10% (meaning that the magnitude of the corrected value is 10% smaller than the magnitude of the uncorrected value). At lower angles of attack, the effects are correspondingly smaller (for example, ≈ 6% at 10-deg angle of attack for the rectangular wing of AR 2.00).

The Kline–McClintock[28] technique for error propagation was used to evaluate all uncertainties in the aerodynamic coefficients. Percentage uncertainties are on the order of 5% for C_L, C_D, and C_M. The uncertainty in the angle of attack was determined to be of the order of ±0.5–0.7 deg for most test cases. Tests of the repeatability of the data presented in this paper showed that all data were repeatable within the uncertainty bounds described earlier.

III. Experimental Results and Discussion

A. General Observations

A complete set of wind-tunnel data is available in Ref. 24. This section lists the most significant characteristics of LAR wing aerodynamics at low Reynolds number and includes a small selection of plots (Figs. 3–21) to illustrate the observations:

1) Wings of aspect ratio below 1.25 have highly nonlinear lift curves that are characterized by high values of $\alpha_{C_{L_{\max}}}$ and nonconstant lift-curve slopes. (Figure 3 is shown as an example corresponding to the rectangular planform of aspect ratios between 0.5 and 2.00.)

2) Above an aspect ratio of 1.25, most of the planforms exhibit lift curves that are more linear. As predicted by theory, the higher the aspect ratio, the more linear the relationship between lift and angle of attack.

3) For aspect ratios below 1.00, a performance advantage is seen for the rectangular, inverse Zimmerman, and elliptical planforms over the Zimmerman planform at angles of attack greater than 15 deg. An example of this is shown in the C_L vs C_D plot (Fig. 4) for an aspect ratio of 0.75.

4) Above an aspect ratio of 1.50, the difference between planforms becomes less clear. For the higher aspect ratios, the elliptical planform is seen to be more efficient (higher lift with lower drag) than the other planforms. This observation is an indication that as the aspect ratio increases, classical aerodynamic theories become effective, especially in terms of the higher efficiency of elliptical planforms.

5) Aspect ratio is by far the most important parameter affecting the aerodynamic characteristics of LAR wings at low Reynolds

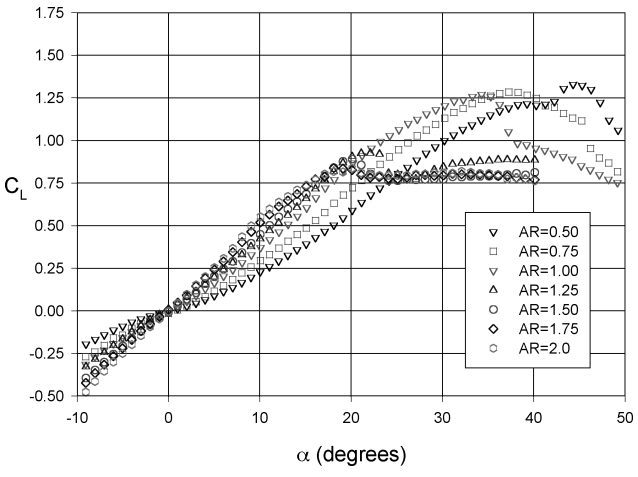

Fig. 3 C_L vs α for rectangular planforms, $Re = 1 \times 10^5$.

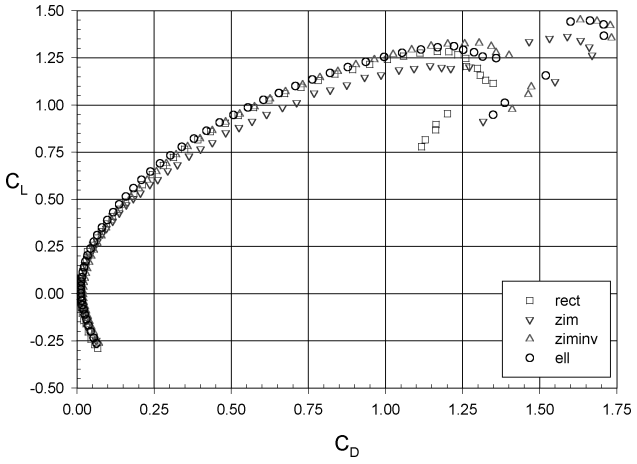

Fig. 4 C_L vs C_D for all planforms at $AR = 0.75$, $Re = 1 \times 10^5$.

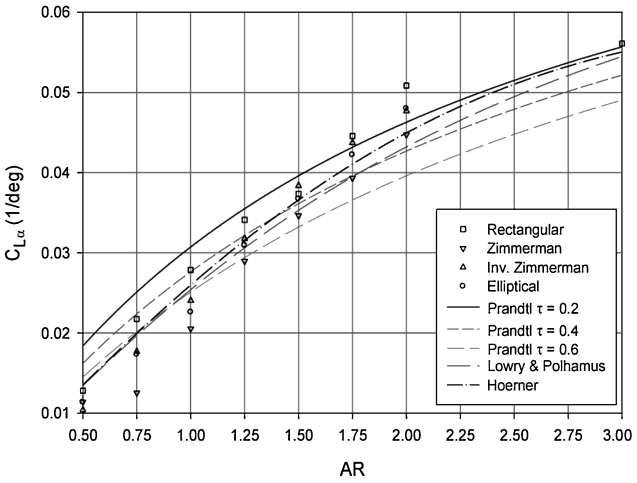

Fig. 5 Average lift-curve slope, C_{L_α} vs AR.

number. Wing planform is the next most important factor, followed by Reynolds number.

6) Hysteresis was not found to be present for any of the measurements shown in this work. It is expected that the low thickness-to-chord ratio of the wings considered is responsible for the absence of hysteresis.

B. Lift Performance: Lift-Curve Slope

One way to compare the performance of different planforms is to compare their lift-curve slopes. However, the inherently nonlinear characteristics of low aspect ratio wings make the definition of a lift-curve slope difficult. Rather than the assumption of a linear relationship, a value for C_{L_α} was calculated by first fitting (in a least-square sense) a second-degree polynomial to the data of lift coefficient vs angle of attack for α below $\alpha_{C_{L_{\max}}}$. The first derivative of this polynomial with respect to angle of attack evaluated at $\alpha = 0$ deg is used to define C_{L_α}.

The values of C_{L_α} were compared with a number of theoretical predictions of the lift-curve slope. The first one is the classic equation for C_{L_α} originating from Prandtl's lifting line theory:

$$C_{L_\alpha} = (1/57.3)\left\{C_{l_\alpha}\Big/\left[1 + \left(C_{l_\alpha}\Big/\pi AR\right)(1+\tau)\right]\right\}(1/\text{deg}) \quad (1)$$

where the Glauert parameter τ, is equivalent to an efficiency factor. The value of C_{l_α} was taken to be $C_{l_\alpha} = 5.3743(1/\text{rad})$ based on the average of experimentally determined two-dimensional slopes of flat-plate infinite wings with the same thickness to chord ratio and leading-edge shape as the wings used in this work.[17]

The second equation used is that discussed by Lowry and Polhamus,[29] which is proposed to be more accurate for small aspect ratios (less than 2):

$$C_{L_\alpha} = \left(\frac{1}{57.3}\right)\frac{2\pi AR}{2 + \sqrt{(AR^2/\eta^2)\left(1 + \tan^2 \Lambda_{c/2}\right) + 4}}\left(\frac{1}{\text{deg}}\right) \quad (2)$$

where $\eta = C_{l_\alpha}/2\pi$, and $\Lambda_{c/2}$ is the sweep angle at midchord.

Finally, Hoerner and Borst[16] suggest that for thin rectangular plates of low AR (less than 2.5), the lift-curve slope is given by

$$C_{L_\alpha} = [36.5/AR + 2AR]^{-1} \quad (3)$$

Values of C_{L_α} at a Reynolds number of 1×10^5 are plotted vs AR in Fig. 5. Figure 5 also includes data from Pelletier and Mueller[17] for an aspect ratio 3.0 rectangular wing model. The approximations of Eqs. (1–3) are also included. [For the curve of Eq. (2), a sweep angle of 0 deg was used.]

From Fig. 5, it can be concluded that no single theoretical equation can accurately model the lift-curve slope of LAR wings at low Reynolds number. The closest agreement is seen to correspond to Hoerner's LAR empirical relationship. Equation (1) with $\tau = 0.2$ or 0.4 also gives relatively good agreement. However, note that the relationship between lift-curve slope and aspect ratio is almost linear in nature and differs in character from the theoretical approximations. One possible explanation for this difference is the way in which lift-curve slope is defined. As described earlier, C_{L_α} is defined as the first derivative of a quadratic equation that is a best fit to the data of lift coefficient vs angle of attack. If a straight line was fitted to the data instead, the value of the slope would be larger, especially for LARs, and would yield a better match between theory and experiment. This discrepancy underscores the fact that it is of limited value to apply an inherently linear theoretical model to the nonlinear aerodynamic characteristics of LAR wings. Other methods should be considered for a more complete analysis. (See next section.)

C. Approximations of Lift, Drag, and Moment Through Nonlinear Equations

The so-called leading-edge-suction analogy was adapted by Polhamus[20,21] for use in LAR wings (mostly of delta planforms). His method assumed that for delta wings in which the flow is mostly attached (before stall), the total force on the wing associated with the pressure required to stabilize the separated vortex cores is equivalent to the leading-edge-suction force required to keep the flow around the sharp leading edges of the wing attached. Polhamus assumed that the leading-edge-suction force acts in a direction normal to the plane of the wing and, thus, gives rise to additional lift associated with the vortices. Using this assumption, he concluded that the total force on a delta wing at moderately high angles of attack before stall is given by an addition of potential lift (calculated from any linear lifting-surface theory) and a vortex lift associated with the leading-edge-suction force. He suggested the following equation for lift coefficient:

$$C_L = K_p \sin\alpha \cos^2\alpha + K_v \cos\alpha \sin^2\alpha \quad (4)$$

where K_p is a factor that depends on the aspect ratio, sweep angle, and leading-edge shape of the wing. K_v is a mostly constant factor approximately equal to π. Comparison of this equation with experimental data for delta wings gives remarkably accurate predictions for lift but rely heavily on the empirical factors K_p and K_v.

Lamar[22,23] extended Polhamus's method to LAR wings of non-delta planforms by taking into account the influence of the side edges. Lamar considered the existence of a force analogous to the leading-edge-suction force that acts at the side edges as the vortex cores roll up onto the upper side of the wing. Following the reasoning of Polhamus, Lamar deduced that the side-edge-suction force also acts in the direction normal to the plane of the wing and, therefore, contributes to vortex lift. A modified lifting-surface theory is used by the author to estimate the relative contributions to the lift force of the leading and side edges, and these coefficients are then used, in a form analogous to Polhamus's equation, to represent the vortex lift of the wing.

It is possible to make use of these nonlinear equations to approximate the experimental data for LAR wings operating at low

Reynolds numbers. The goal of this section is to provide the reader with empirically determined constants that, when applied to the nonlinear equations presented hereafter, will generate approximate curves of lift, drag, and pitching moment as a function of angle of attack, aspect ratio, and wing planform.

The following equations are used for the approximate curves of lift, drag, and moment.

1. Lift

The Polhamus equation is used for approximating the lift coefficient:

$$C_L = K_p \sin\alpha \cos^2\alpha + K_v \cos\alpha \sin^2\alpha \tag{5}$$

Even though Lamar's analysis shows that K_v varies slightly as a function of aspect ratio and planform, it was found in the present analysis that very good agreement with experimental data could be achieved if K_v is set constant. This simplification reduces the number of parameters required to recreate the LAR wing aerodynamic data. Therefore, in this paper, K_v is set equal to π.

2. Drag

A nonlinear equation for the drag coefficient as a function of angle of attack was proposed by Lamar:

$$C_D = C_{D_0} + K_p \sin^2\alpha \cos\alpha + K_v \sin^3\alpha \tag{6}$$

It was found, however, that agreement with the experimental data was not very good. A much better agreement was found to exist by the use of the classical equation for induced drag:

$$C_D = C_{D_0} + K[C_L]^2 \tag{7}$$

where K is the induced drag factor, a function of aspect ratio, planform, and leading-edge geometry.

3. Pitching Moment

Lamar's nonlinear equation for the pitching moment about the leading edge is

$$(C_M)_{\text{LE}} = x_p K_p \sin\alpha \cos\alpha + x_e K_v \sin^2\alpha \tag{8}$$

where x_p is the location along the chordwise direction at which the potential (linear) lift is assumed to be acting, normalized by the mean aerodynamic chord. Similarly, x_e is the location at which the nonlinear lift is assumed to act, again normalized by the chord. Note that in the Polhamus/Lamar analogy, the nonlinear lift is considered to be generated by the leading and side edges, which explains the use of the e subscript for edge. In the present analysis, x_p is taken to correspond to the 25% chord location with respect to the MAC, and it is, therefore, set to $x_p = 0.25$. Here x_e remains as the equation parameter.

The experimental data for the LAR wings presented in this work were used to calculate values for the parameters in Eqs. (5), (7), and (8) that best fit the data. This was accomplished by iteratively finding the parameters that minimized the sum of the squares of the errors between the experimental data and the result obtained through the nonlinear equations. This procedure was applied for each of the four planforms and for each of the seven aspect ratios studied in this work. The nonlinear equation approximations are only applicable up to the angles of attack shown in Fig. 6. At greater values of α, the highly nonlinear effects associated with prestall and stall conditions cannot be modeled accurately by the equations.

Figure 7 shows a typical comparison of the experimental data and Eqs. (5), (7), and (8) for the rectangular planform of aspect ratio 1.00. Curves for other aspect ratios and planforms are similar in terms of the ability of the equations to approximate the data. Figures 8 and 9 show comparisons of only the lift curve for all planforms and for aspect ratios between 0.75 and 2.00. Again, agreement between experiment and theory is seen to be good for all aspect ratios.

Figures 10–12 show the optimum values of K_p, K, and x_e for each of the planforms and aspect ratios. Figure 10 reveals that the K_p values for the Zimmerman planform for aspect ratios below 1.25 are noticeably lower than those of the rectangular or inverse Zimmerman planform. This once again points to the conclusion that the Zimmerman planform has lower lift performance for low AR. Above an AR of 1.5, the difference between the planforms becomes less drastic, but the Zimmerman planform still has a lower value of K_p.

The plot for induced drag parameter K (Fig. 11) shows that as the aspect ratio increases, the induced drag factor decreases, as would be expected from linear theory. Differences between planforms are not as pronounced as in the K_p case; nevertheless, for lower aspect ratios, the Zimmerman planform's K value is generally higher than the other planforms. In terms of C_{D_0}, the uncertainty in the data for the very low values of C_{D_0} indicates no clear trend of this parameter with respect to aspect ratio or planform. The average value of C_{D_0} for all wings was found to be approximately 0.015.

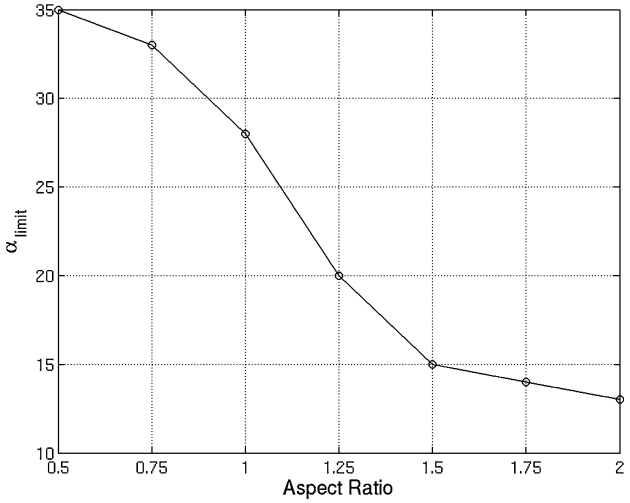

Fig. 6 Highest angle of attack for applicability of nonlinear equations.

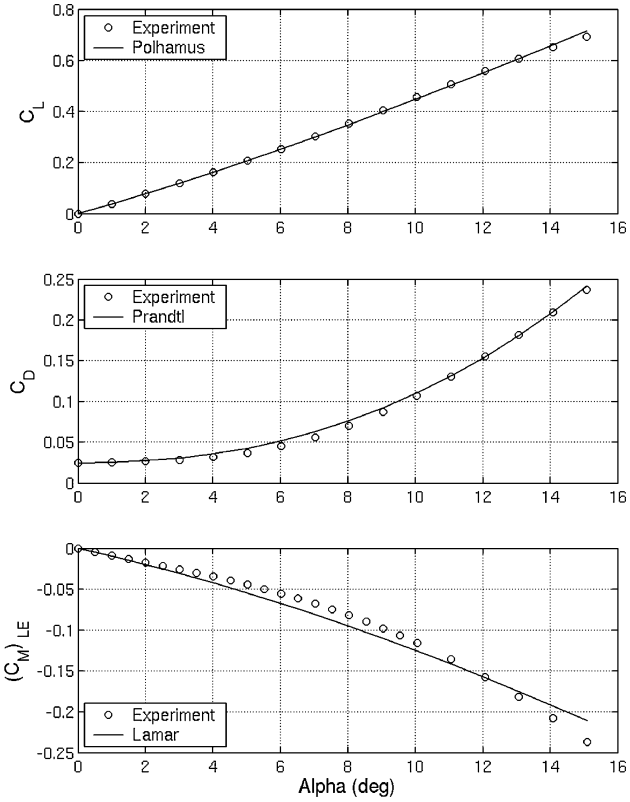

Fig. 7 Comparison with nonlinear equations: rectangular AR = 1.00, $Re = 1 \times 10^5$.

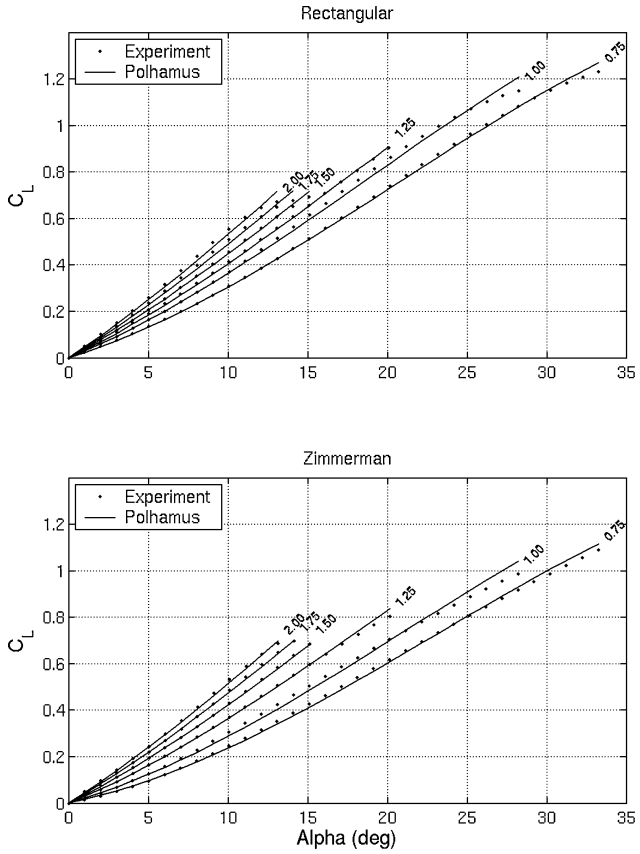

Fig. 8 Lift comparison with nonlinear equations: rectangular and Zimmerman planforms, $Re = 1 \times 10^5$.

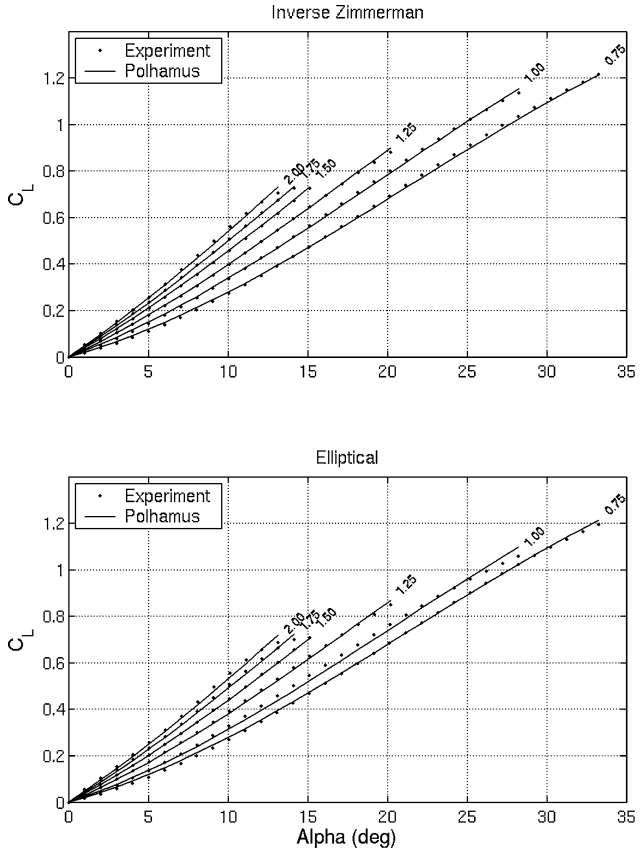

Fig. 9 Lift comparison with nonlinear equations: inverse Zimmerman and elliptical planforms, $Re = 1 \times 10^5$.

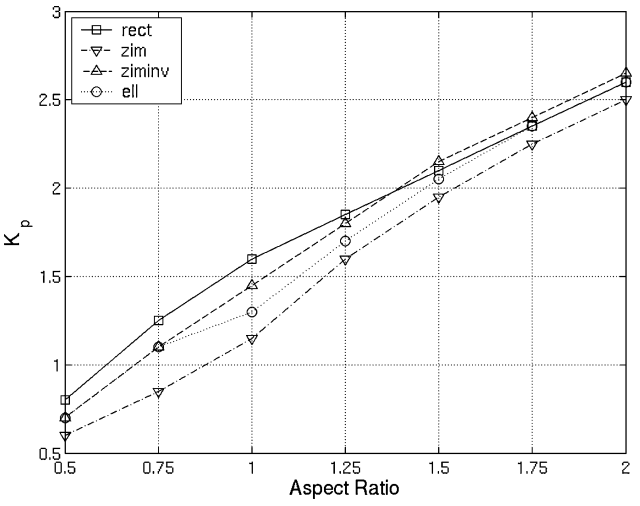

Fig. 10 Parameter K_p vs AR and planform.

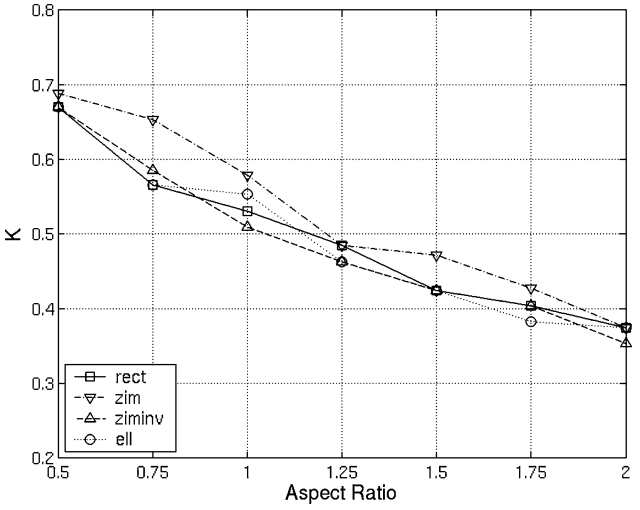

Fig. 11 Parameter K vs AR and planform.

Finally, the plot of moment coefficient parameter x_e can be used as an indicator of the nonlinearity of a given planform (Fig. 12). The parameter x_e corresponds to the location along the chordwise direction at which the nonlinear portion of the lift can be assumed to be acting. Wings with stronger nonlinear lift contributions will have greater values of x_e (Fig. 12). An indication of the same trend will be reinforced by the analysis in Sec. III.E.

D. Maximum Lift Coefficient

An important characteristic of LAR wings is their high value of $C_{L_{\max}}$ and $\alpha_{C_{L_{\max}}}$. Figures 13 and 14 plot the values of $C_{L_{\max}}$ and $\alpha_{C_{L_{\max}}}$ for each of the four planforms as a function of aspect ratio. Note from Figs. 13 and 14 that aspect ratio and wing planform have significant influence in the maximum lift characteristics of LAR wings.

It is evident that a transition zone exists for $C_{L_{\max}}$ and $\alpha_{C_{L_{\max}}}$ in the aspect ratio range between 1.25 and 1.50. The reason for the transition is proposed to be as follows: For wings of aspect ratio below 1.25, as the angle of attack approaches $\alpha_{C_{L_{\max}}}$, the flow induced by the wing-tip vortices is able to energize the flow on the upper surface of the wing and delay the onset of separation. As the aspect ratio increases, however, the strength of the wing-tip vortex flow structures on the upper surface of the wing decreases. Separation for these wings, therefore, occurs at lower angles of attack (and correspondingly lower lift coefficients).

Also note that the aspect ratio at which the transition in the $\alpha_{C_{L_{\max}}}$ curve occurs is dependent on wing planform. The elliptical and

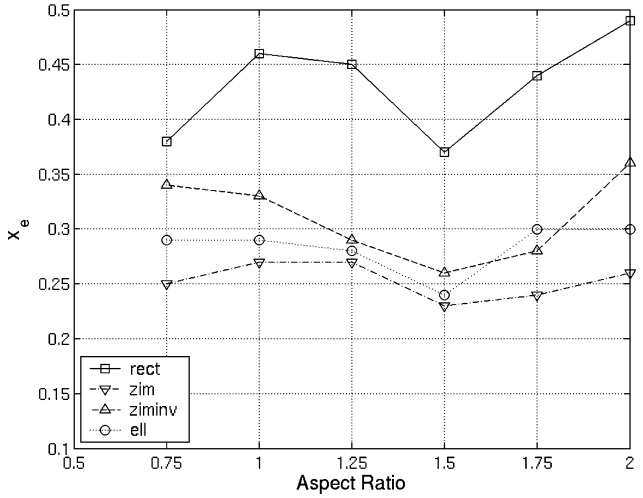

Fig. 12 Parameter x_e vs AR and planform.

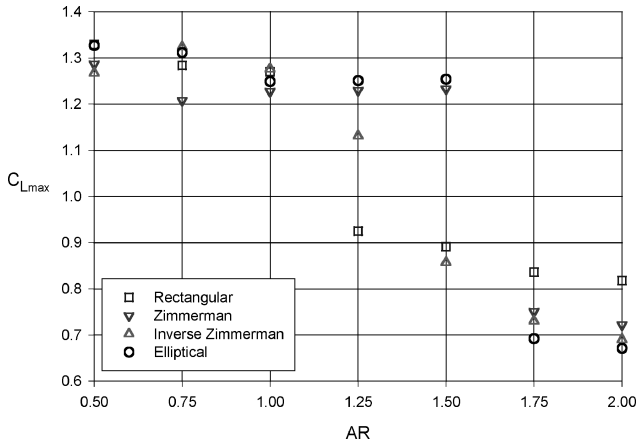

Fig. 13 $C_{L_{max}}$ of four wing planforms and all aspect ratios ($Re = 1 \times 10^5$).

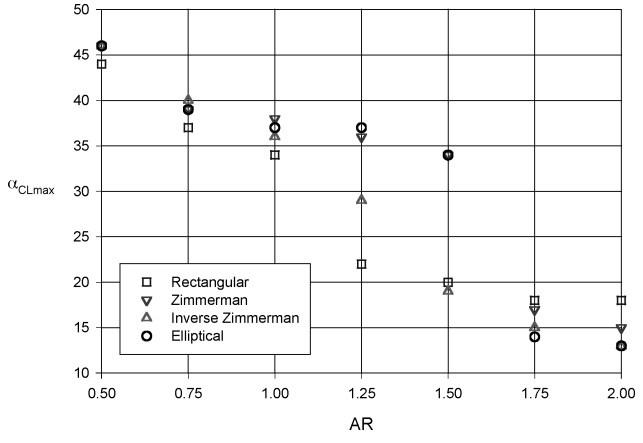

Fig. 14 Four wing planforms and all aspect ratios of $\alpha_{C_{L_{max}}}$ ($Re = 1 \times 10^5$).

Zimmerman wings have higher values of $C_{L_{max}}$ and $\alpha_{C_{L_{max}}}$ than the rectangular and inverse Zimmerman wings for AR = 1.50. One possible explanation for the difference between planforms is based on the fact that for wings of high aspect ratio, the mechanism responsible for lift generation near $\alpha_{C_{L_{max}}}$ is highly dependent on the shape and planform geometry of the leading edge. The empirical/theoretical analysis proposed in DATCOM[30] was applied to this problem. (See Torres[24] for details.) It was concluded that for aspect ratios above 1.50, the predicted values of $\alpha_{C_{L_{max}}}$ were higher for elliptical and Zimmerman wings than for the other two planforms. It is likely that in the transition region of $C_{L_{max}}$ and $\alpha_{C_{L_{max}}}$, the leading-edge planform geometry of elliptical and Zimmerman wings is responsible for delaying the onset of separation. Nevertheless, the structure of the flow near $\alpha_{C_{L_{max}}}$ for LAR wings at low Reynolds numbers is highly complex. Many flow mechanisms may be interacting in this regime.

E. Center of Lift

One key aspect of LAR wing aerodynamics is the location of the center of lift (or center of pressure) as a function of wing planform, aspect ratio, and angle of attack. The center of lift location yields important information about the nature of LAR wing aerodynamics, especially in the nonlinear lift regime.

The location of the center of lift can be calculated by the use of sting balance data of normal force and pitching moment taken about the $\bar{c}/4$ location of each wing. For this purpose, the parameter h_{CL} is defined as the distance between the leading edge of $\bar{c}$ and the center of pressure, divided by $\bar{c}$ ($h_{\mathrm{CL}} = x_{\mathrm{CL}}/\bar{c}$). If the procedure outlined by Torres[24] is followed, a value of h_{CL} is calculated for each wing and aspect ratio at each angle of attack. The uncertainty in the value of h_{CL} was found to vary between 6% of h_{CL} for angles of attack close to 0 deg and 4% of h_{CL} for angles of attack above 15 deg.

Figures 15–21 provide great insight into the lift-generating mechanisms that operate in the regime of LAR wings at low Reynolds number. The most striking observation is the drastic shift in the location of the center of lift as angle of attack increases. As an example, consider the rectangular wing of AR = 1.00, shown in Fig. 15. For this wing, h_{CL} is close to 0.17 at $\alpha = 0$ deg but increases to 0.40 at $\alpha = 40$ deg. It can be concluded that the chordwise location at which the lift force is acting shifts downstream as the angle

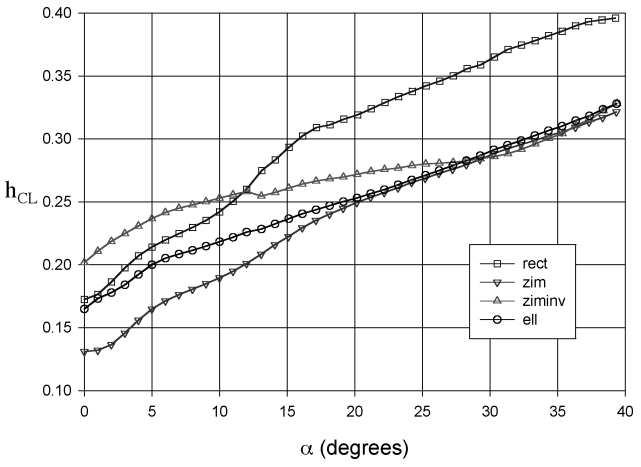

Fig. 15 Location of center of lift h_{CL} vs α: AR = 1.00 and $Re = 1.4 \times 10^5$.

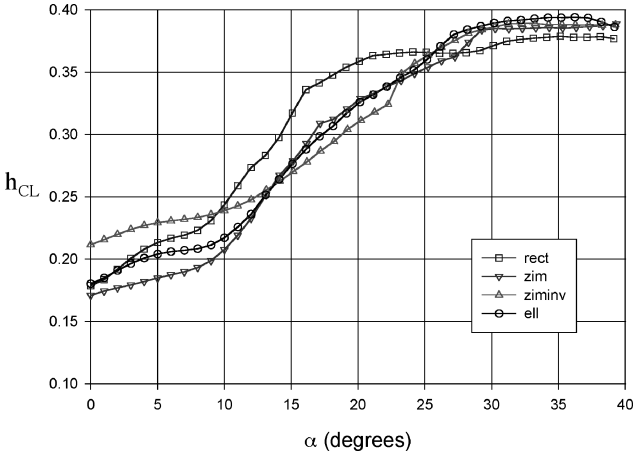

Fig. 16 Location of center of lift h_{CL} vs α: AR = 1.50 and $Re = 1.4 \times 10^5$.

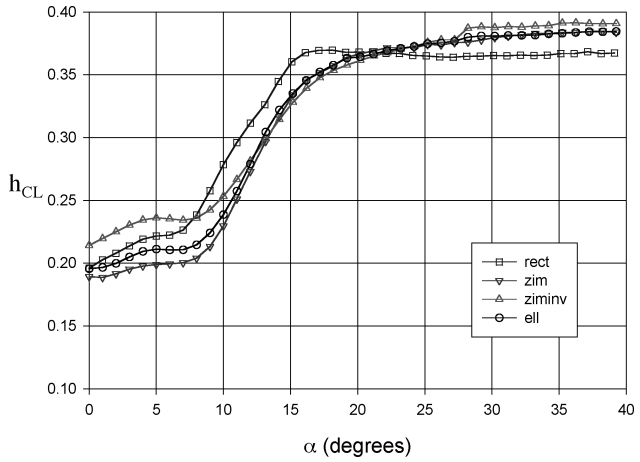

Fig. 17 Location of center of lift h_{CL} vs α: AR = 2.00 and $Re = 1.4 \times 10^5$.

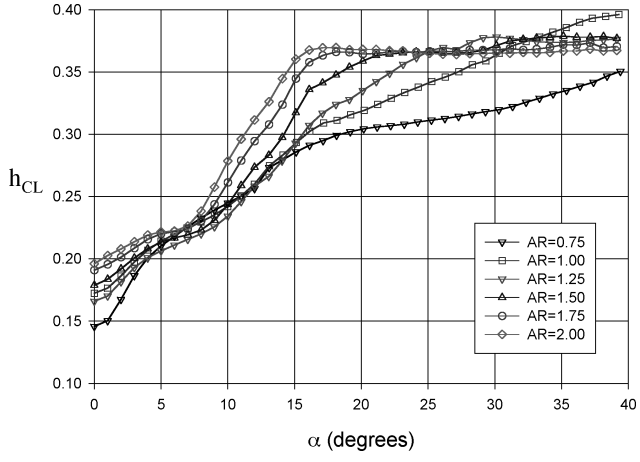

Fig. 18 Location of center of lift h_{CL} vs α: rectangular planform and $Re = 1.4 \times 10^5$.

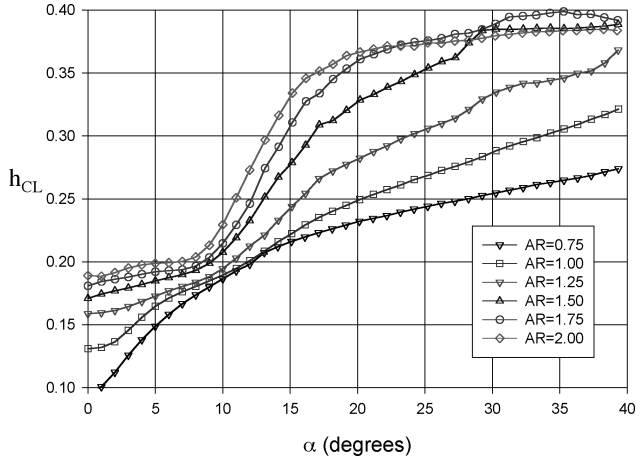

Fig. 19 Location of center of lift h_{CL} vs α: Zimmerman planform and $Re = 1.4 \times 10^5$.

of attack increases. This is an expected trend based on the linear–nonlinear theory of LAR wings. For low angles of attack, most of the lift generated by the wing is in the form of circulation lift, as seen in wings of high aspect ratio. Therefore, it is expected that the location of the center of lift will be close to the 25%-chord location at these angles. However, as the angle of attack increases, the lift mechanism shifts to that generated by the wing-tip vortices. These vortices generate lift by creating low-pressure sections on the upper surface of the wing, usually more on the downstream end of the

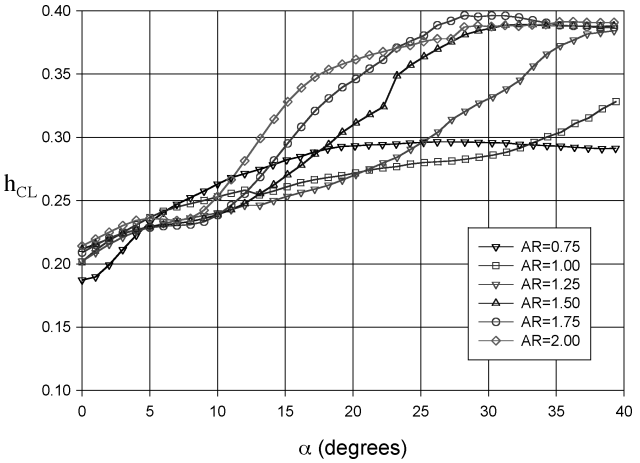

Fig. 20 Location of center of lift h_{CL} vs α: inverse Zimmerman planform and $Re = 1.4 \times 10^5$.

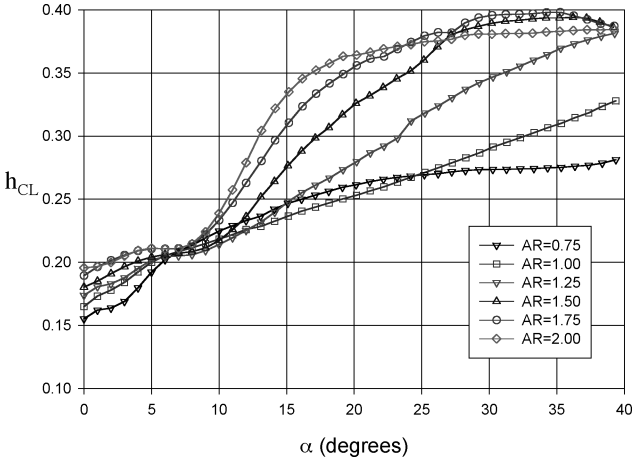

Fig. 21 Location of center of lift h_{CL} vs α: elliptical planform $Re = 1.4 \times 10^5$.

wing. (The wing-tip vortices increase in size and strength as they travel downstream along the upper surface of the wing.) It would be expected that because the lift generated at higher angles of attack is due to wing-tip vortices (which are stronger near the trailing edge), the location of the center of lift would shift downstream. The amount by which the center of lift shifts toward the trailing edge is a direct indication of how much nonlinear lift is being generated by the wing. Wings of $AR = 0.75$ have a much steeper shift of center of lift with α than wings of $AR = 2.00$. If one were to plot h_{CL} vs α for a wing of $AR = 10.00$, this curve would be expected to be a horizontal line centered close to 0.25. Until $\alpha_{C_{L_{max}}}$ is reached, h_{CL} would not be expected to change.

Another important conclusion that can be drawn from the center of lift analysis relates to the effect of planform and how some planforms are more linear than others. Zimmerman and elliptical planforms are seen to have a value of h_{CL} that is generally lower than that of rectangular and inverse Zimmerman planforms. This is probably due to the fact that Zimmerman and elliptical planforms have a weaker wing-tip vortex system than the one found in inverse Zimmerman and rectangular planforms. As such, it would be expected that the center of lift of the planforms with the weaker vortices would be farther forward than the center of lift of wings with strong vortices. This is indeed the case.

IV. Conclusions

The aerodynamic characteristics of wings of aspect ratio between 0.5 and 2.0 were experimentally determined at Reynolds numbers below 2×10^5. Of primary interest in this study were the effects of wing planform and aspect ratio on the forces and moments of LAR

wings at low Reynolds numbers. Results showed large nonlinearities in the lift curves, especially for aspect ratios below 1.25. Wings of such LARs were also found to have high values of maximum lift coefficient and corresponding angle of attack.

Wing planform was determined to have significant aerodynamic effects. Wings of inverse Zimmerman planforms were found to be more efficient than other planforms for aspect ratios below 1.0 and high angles of attack. For higher values of AR, elliptical planforms were found to yield more favorable characteristics, especially at low to moderate angles of attack.

Additional analysis of the aerodynamic data revealed that analytical expressions for the lift-curve slope are not very accurate over the entire range of aspect ratios and planforms. Efficiency factors of 50–80% were found to give the best agreement with lifting-line-theory-based expressions. Comparison of wind-tunnel data with nonlinear equations for lift, drag, and moment coefficient showed that, up to moderate angles of attack, the nonlinear equations modeled the experimental data quite well, provided that the right equation parameters were used. Optimum values of the parameters to be used in these equations were determined and plotted as functions of aspect ratio and planform.

With respect to performance near $\alpha_{C_{L_{\max}}}$, it was found that a transition exists in the curves of $C_{L_{\max}}$ and $\alpha_{C_{L_{\max}}}$ vs aspect ratio. This transition, which occurs near $AR = 1.25$, provides an indication of the transition between nonlinear and linear lift generation mechanisms at high angles of attack near stall. It was also noted that rectangular/inverse Zimmerman planforms and elliptical/Zimmerman wings have drastically different values of $C_{L_{\max}}$ and $\alpha_{C_{L_{\max}}}$ for an aspect ratio of 1.50. A probable reason for this difference is proposed to be related to the planform geometry of the leading edge of elliptical and Zimmerman wings.

The location of the center of lift as a function of planform, aspect ratio, and angle of attack was determined by the use of wind-tunnel data. This analysis provided great insight into the linear–nonlinear lift character of LAR wings. The location of the center of lift was found to shift toward the trailing edge of the wing as the angle of attack increased. It was proposed that the reason for this shift is related to the nonlinear lift generated by the wing-tip vortices, which are more dominant in the aft section of the wing.

References

[1]Foch, R. J., Dahlburg, J. P., McMains, J. W., Bovais, C. S., Carruthers, S. L., Cole, R., Gardner, J. H., Kellogg, J. C., Schuette, L. C., and Tayman, S. K., "Dragon Eye, an Airborne Sensor System for Small Units," *Proceedings of AUVSI Unmanned Systems Conference and Exhibition*, Association for Unmanned Vehicle Systems International, Arlington, VA, 2000, pp. 1–13.

[2]Hoffman, C., "Aero Boy," *Popular Science*, Vol. 262, No. 6, 2003, pp. 52–59.

[3]Dornheim, M. A., "Tiny Drones May Be Soldier's New Tool," *Aviation Week and Space Technology*, Vol. 148, No. 23, 1998, pp. 42–48.

[4]Grasmeyer, J. M., and Keennon, M. T., "Development of the Black Widow Micro Air Vehicle," *Fixed and Flapping Wing Aerodynamics for micro Air Vehicle Applications*, edited by T. J. Mueller, Vol. 195, Progress in Astronautics and Aeronautics, AIAA, Reston, VA, 2001.

[5]Fulghum, D. A., "Miniature Air Vehicles Fly into Army's Future," *Aviation Week and Space Technology*, 9 Nov. 1998, p. 37.

[6]Kellogg, J., Bovais, G., Dahlburg, J., Foch, R., Gardner, J., Gordan, D., Hartley, R., Kamgar-Parsi, B., McFarlane, H., Pipitone, F., Ramamurthi, R., Sciambi, A., Spears, W., Srull, D., and Sullivan, C., "The NRL Mite Air Vehicle," *Proceedings of the 16th International Conference on Unmanned Air Vehicle Systems*, Bristol, England, U.K., 2001, pp. 25-1–25-14.

[7]Shyy, W., Berg, M., and Ljungqvist, D., "Flapping and Flexible Wings for Biological and Micro Air Vehicles," *Progress in Aerospace Sciences*, Vol. 35, 1999, pp. 455–505.

[8]Zimmerman, C. H., "Characteristics of Clark Y airfoils of Small Aspect Ratios," NACA TR 431, 1932.

[9]Winter, H., "Flow Phenomena on Plates and Airfoils of Short Span," NACA TM 798, July 1936.

[10]Flax, A. H., and Lawrence, H. R., "The Aerodynamics of Low-Aspect-Ratio Wings and Wing–Body Combinations," *Third Anglo-American Aeronautical Conference*, Royal Aeronautical Society, London, 1952, pp. 363–398.

[11]Bartlett, G. E., and Vidal, R. J., "Experimental Investigation of Influence of Edge Shape on the Aerodynamic Characteristics of Low-Aspect-Ratio Wings at Low Speeds," *Journal of the Aeronautical Sciences*, Vol. 22, No. 8, 1995, pp. 517–533.

[12]Wadlin, K. L., Ramsen, J. A., and Vaughan, V. L., Jr., "The Hydrodynamic Characteristics of Modified Rectangular Flat Plates Having Aspect Ratios of 1.00, 0.25, and 0.125 and Operating Near a Free Water Surface," NACA TR 1246, 1955.

[13]Gersten, K., "Calculation of Non-Linear Aerodynamic Stability Derivatives of Aeroplanes," Technical Rept. 342, AGARD, April 1961.

[14]Bradley, R. G., Smith, C. W., and Bhateley, I. C., "Vortex-Lift Prediction for Complex Wing Planforms," *Journal of Aircraft*, Vol. 10, No. 6, 1973, pp. 379–381.

[15]Hoerner, S. F., *Fluid-Dynamic Drag*, Hoerner Fluid Dynamics, Brick Town, NJ, 1965, Chap. 7.

[16]Hoerner, S. F., and Borst, H. V., *Fluid-Dynamic Lift*, Hoerner Fluid Dynamics, Brick Town, NJ, 1975, pp. 9-8, 9-9, 17-5, and 20-8.

[17]Pelletier, A., and Mueller, T. J., "Low Reynolds Number Aerodynamics of Low-Aspect-Ratio," Thin/Flat/Cambered-Plate Wings," *Journal of Aircraft*, Vol. 37, No. 5, 2000, pp. 825–832.

[18]Bollay, W., "A Non-Linear Wing Theory and Its Application to Rectangular Wings of Small Aspect Ratio," *Zeitschrift Fur Angewandte Mathematik und Mechanik*, Vol. 19, 1939, pp. 21–35.

[19]Belotserkovskii, S. M., "Calculation of the Flow About Wings of Arbitrary Planform at a Wide Range of Angles of Attack," Royal Aircraft Establishment, Technical Rept. Library Translation 1433, London, Feb. 1970.

[20]Polhamus, E. C., "A Concept of the Vortex Lift of Sharp-Edge Delta Wings Based on a Leading-Edge-Suction Analogy," NASA TN D-3767, 1966.

[21]Polhamus, E. C., "Predictions of Vortex-Lift Characteristics by a Leading-Edge-Suction Analogy," *Journal of Aircraft*, Vol. 8, No. 4, 1971, pp. 193–199.

[22]Lamar, J. E., "Extension of Leading-Edge-Suction Analogy to Wings with Separated Flow Around the Side Edges at Subsonic Speeds," NASA TR R-428, 1974.

[23]Lamar, J. E., "Prediction of Vortex Flow Characteristics of Wings at Subsonic and Supersonic Speeds," *Journal of Aircraft*, Vol. 13, No. 7, 1976, pp. 490–494.

[24]Torres, G. E., "Aerodynamics of Low Aspect Ratio Wings at Low Reynolds Numbers with Applications to Micro Air Vehicle Design," Ph.D. Dissertation, Dept. of Aerospace and Mechanical Engineering, Univ. of Notre Dame, Notre Dame, IN, 2002.

[25]Zimmerman, C. H., "Aerodynamic Characteristics of Several Airfoils of Low Aspect Ratio," NACA TN 539, 1935.

[26]Pankhurst, R. C., and Holder, D. W., *Wind-Tunnel Technique*, Sir Isaac Pitman and Sons, London, 1952, Chap. 8.

[27]Barlow, J. B., Rae, X., and Pope, X., *Low-Speed Wind Tunnel Testing*, Wiley, New York, 1999, Chap. 10.

[28]Kline, S. J., and McClintock, F. A., "Describing Uncertainties in Single-Sample Experiments," *Mechanical Engineering*, Vol. 75, No. 1, 1953, pp. 3–8.

[29]Lowry, J. G., and Polhamus, E. C., "A Method for Predicting Lift Increments due to Flap Deflection at Low Angles of Attack in Incompressible Flow," NACA TN 3911, 1957.

[30]Hoak, D. E., and Finck, R. D., *U.S.A.F Stability and Control DATCOM*, Global Engineering Documents, Englewood, CO, 1978, Secs. 2.1, 2.2, and 4.8.

W. Devenport
Associate Editor